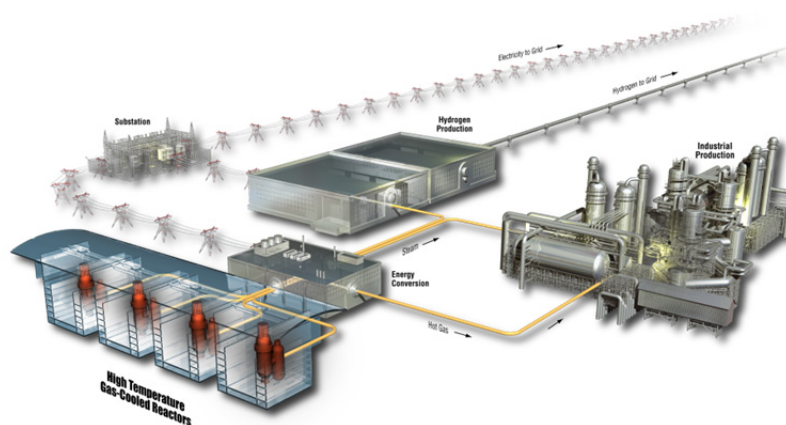


AGR-1, AGR-2 and AGR-3/4 Dimensional Change Data Analysis

Sarah E. Herberger

February 2016

The INL is a
U.S. Department of Energy
National Laboratory
operated by
Battelle Energy Alliance



DISCLAIMER

This information was prepared as an account of work sponsored by an agency of the U.S. Government. Neither the U.S. Government nor any agency thereof, nor any of their employees, makes any warranty, expressed or implied, or assumes any legal liability or responsibility for the accuracy, completeness, or usefulness, of any information, apparatus, product, or process disclosed, or represents that its use would not infringe privately owned rights. References herein to any specific commercial product, process, or service by trade name, trade mark, manufacturer, or otherwise, does not necessarily constitute or imply its endorsement, recommendation, or favoring by the U.S. Government or any agency thereof. The views and opinions of authors expressed herein do not necessarily state or reflect those of the U.S. Government or any agency thereof.

AGR-1, AGR-2 and AGR-3/4 Dimensional Change Data Analysis

Sarah E. Herberger

February 2016

**Idaho National Laboratory
INL ART TDO Program
Idaho Falls, Idaho 83415**

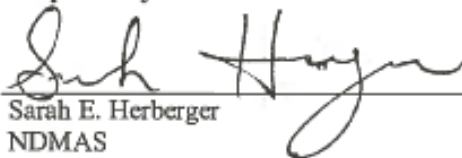
INL ART TDO Program

AGR-1, AGR-2 and AGR-3/4 Dimensional Change Data Analysis

INL/EXT-16-37916
Revision 0


February 2016

Prepared by:


Sarah E. Herberger
NDMAS

2/26/2016
Date

Approved by:


Nancy J. Lybeck
NDMAS Technical Lead

2-26-2016
Date


Jeffrey J. Emerson
Human Factors, Controls & Statistics Manager

2-29-2016
Date


Paul A. Demkowicz
INL ART TRISO Fuel Technical Lead

2/26/16
Date


Michelle T. Sharp
INL ART TDO Quality Assurance

2/29/16
Date

ABSTRACT

A series of Advanced Gas Reactor (AGR) experiments have been completed in the Advanced Test Reactor at Idaho National Laboratory in support of qualification and development of tristructural isotropic fuel. Each AGR test consists of multiple independently controlled and monitored capsules containing fuel compacts placed in a graphite cylinder. These capsules are instrumented with thermocouples embedded in the graphite, enabling temperature control. The fuel compacts are composed of fuel particles surrounded by a graphitic A3 matrix material. Dimensional change in AGR fuel compacts is vital because the swelling or shrinkage affects the size of the gas gaps that are used to control temperatures. Analysis of dimensional change in the AGR fuel compacts is needed to establish the variables directly relating to compact shrinkage.

The variables initially identified for consideration were matrix density, compact density, fuel packing fraction, uranium loading, fuel particle diameter, cumulative fast neutron fluence, and volume average time average fuel temperature. In addition to the data available from the AGR experiments, the analysis included specimens formed from the same A3 matrix material used in Advanced Graphite Creep (AGC) experiments, which provide graphite creep data during irradiation for design and licensing purposes. The primary purpose of including the AGC specimens was to encompass dimensional behavior at zero packing fraction, zero uranium loading, and zero particle diameter.

All possible combinations of first order variable regressions were considered in the analysis. The study focused on identifying the best regression models for percent change in diameter, length, and volume. Bootstrap analysis was used to ensure the resulting regression models were robust and well-performing. The variables identified as very significant in predicting change in one or more dimensions (diameter, length, and volume) are volume average time average temperature, fast fluence, compact density, packing fraction and fuel particle diameter. Due to the presence of confounding effects between several variables, interpretation of these results is equivocal; the use of multiple statistical tests provides additional confidence in the conclusion.

CONTENTS

ABSTRACT.....	vii
ACRONYMS.....	xi
1. INTRODUCTION.....	1
2. EXPERIMENTAL DESIGN.....	2
3. DATA.....	4
3.1 Compact Diameter	4
3.2 Compact Length.....	6
3.3 Compact Volume	6
3.4 Compact Explanatory Variables	7
4. ANALYSIS	8
4.1 Change in Compact Diameter	9
4.2 Change in Compact Length.....	11
4.3 Change in Compact Volume	14
5. CONCLUSION AND DISCUSSION	16
6. REFERENCES	17

FIGURES

Figure 1. AGR-1 test train axial schematic (left) and radial cross section of a capsule (right).	2
Figure 2. AGR-3/4 axial schematic (left) and radial cut of a capsule (right)......	3
Figure 3. AGC-2 graphite compacts axial schematic (top) and radial cross section of a capsule (bottom).	4
Figure 4. FAB and PIE diameter box plot for compacts included in this analysis by experiment.	5
Figure 5. Observed regressed by predicted percent change in diameter by compact.	11
Figure 6. Observed plotted against predicted natural log of the transformed percent change in length.	14
Figure 7. The observed by predicted natural log of percent change in volume.	15

TABLES

Table 1. Summary statistics for measured FAB and PIE compact diameters included in this analysis by experiment. “N” represents the number of compacts analyzed from each experiment.	5
Table 2. Summary statistics for measured FAB and PIE compact lengths based on the compacts included in this analysis. “N” represents the number of compacts analyzed from each experiment.	6
Table 3. Summary statistics for calculated FAB and PIE compact volume across experiments included in this analysis. “N” represents the number of compacts analyzed from each experiment.	7
Table 4. Summary statistics for explanatory variables utilized in the analysis across experiments.	7
Table 5. Results of a Duncan’s Multiple Range Test for percent change in diameter.	10
Table 6. The top-performing regression with four variables, to predict percent change in diameter.	10
Table 7. Results of a Duncan’s Multiple Range Test for percent change in fabricated and post-irradiation examination length.	12
Table 8. The top performing regression with four variables for natural log of the transformed percent change in length.	13
Table 9. The top performing regression with four variables for natural log of percent change in volume.	15
Table 10. Regression coefficients for change in length, diameter, and volume.	16

ACRONYMS

AGC	Advanced Graphite Creep
AGR	Advanced Gas Reactor
ATR	Advanced Test Reactor
DMRT	Duncan's Multiple Range Test
FAB	fabrication
HEXA	hexamethylenetetramine
Hf	hafnium
HTGR	high temperature gas-cooled reactor
INL	Idaho National Laboratory
IPyC	inner pyrolytic carbon
Ln	Natural Log
NDMAS	Nuclear Data Management and Analysis System
OPyC	outer pyrolytic carbon
PIE	post-irradiation examination
SiC	silicon carbide
SST	stainless steel
TRISO	tristructural isotropic
VATAT	Volume Average Time Average Temperature

AGR-1, AGR-2 and AGR-3/4 Dimensional Change Data Analysis

1. INTRODUCTION

A series of fuel irradiation experiments have been conducted in the Advanced Test Reactor (ATR) at Idaho National Laboratory (INL) to support the licensing and operation of the Advanced Reactor Technologies (ART) high temperature gas-cooled reactor (HTGR). The Advanced Gas Reactor (AGR) Fuel Development and Qualification experiments are comprised of multiple independent capsules containing multiple cylindrical fuel compacts, placed inside of a graphite holder in the ATR. The AGR experiments provide data on fuel performance under irradiation and potential accident conditions, support fuel process development, qualify the fuel for normal operating conditions, provide irradiated fuel for potential accident testing, and support the development of fuel performance and fission product transport models.

In parallel, a series of graphite irradiation experiments have been conducted at ATR to support the design of graphite core components for HTGRs. The Advanced Graphite Creep (AGC) experiments use matched pairs of stressed and unstressed graphite specimens to assess the effects of irradiation on dimensional and thermomechanical properties. To date, six irradiation campaigns have been completed: AGR-1 (December 2006–November 2009); AGR-2 (June 2010–October 2013); AGR-3/4 (December 2011–April 2014); AGC-1 (September 2009–January 2011); AGC-2 (April 2011–May 2012); and AGC-3 (November 2012–April 2014).

The fuel compacts in AGR-1, 2, and 3/4 are composed of tristructural-isotropic (TRISO) -coated fuel particles and A3 matrix material. The TRISO spheres are a uranium material mixture encased in buffer, dense inner pyrolytic carbon (IPyC), silicon carbide (SiC), and dense outer pyrolytic carbon (OPyC) layers [1]. The SiC layer provides structural integrity and retains fission products at elevated temperatures. The fuel particles are then pressed into a cylindrical shape with the matrix material filling in the spaces between the TRISO fuel spheres. The TRISO fuel particles are structures that do not change dimensions when irradiated, and their purpose is to contain the fuel. The matrix is composed of resin and graphite; in weight percent the matrix is 80% Asbury and Graphtech graphites, 20% Hexion SD-1708 high purity phenolic resin with 8% Hexa. The matrix is then pressed and heated with the fuel particles to 1800°C, inside of a cylinder form [2].

Graphite composes a majority of the fuel compacts, and has been utilized in the nuclear industry for over 60 years. Graphite is chosen as a moderator in part due to its low coefficient of thermal expansion and its high thermal conductivity, which together provide excellent resistance to thermal shock. Based on the properties of graphite when temperatures greater than 1000°C are reached, the molecular bonds between graphite molecules are strengthened [3]. This additional strength is critical as during irradiation, fast neutrons cause damage to the crystal structure, leading to distortion and cracking of the graphite [4].

Dimensional changes in AGR fuel compacts are important because the swelling or shrinkage affects the size of the gas gaps that are used to control temperatures. Analysis of dimensional changes in the AGR fuel compacts is necessary to establish the significant factors impacting compact shrinkage.

Based on the availability of post-irradiation data, 162 AGR-1, -2, and -3/4 fuel compacts were considered for inclusion in the analysis. Additionally, 17 AGC-2 graphite-only specimens were identified for inclusion in this analysis. These specimens were selected because they were machined from the same graphite matrix material (A3) used in the AGR fuel compacts, were measured post-irradiation, and were not subjected to mechanical stress. For the sake of simplicity, the word compact will be used to collectively refer to both the AGR fuel compacts and the AGC specimens throughout this report. A total of 179 AGC and AGR compacts were initially considered for inclusion in the analysis. Six compacts from

AGR-1 were eliminated from consideration due to significant size and composition differences, resulting in the analysis of 173 AGC and AGR compacts.

2. EXPERIMENTAL DESIGN

For all experimental test trains, the capsule components are given unique identifiers and cataloged to preserve the identity of the component and the location within the test train from which the component was removed. For example, the capsule number, level within the capsule, and stack number were recorded for each compact, along with many irradiation conditions. Each experimental test train had a different setup, which is illustrated in Figure 1 through Figure 3.

The AGR-1 test train was a multi-capsule, instrumented lead experiment, designed for irradiation in the 38.1-mm-diameter B-10 (large B) position of the ATR. The test train contained six capsules, each independently controlled for temperature and independently monitored for fission product gas release. An axial view of the test train is illustrated in Figure 1 (left). Each AGR-1 capsule is 152.4 mm long and contains 12 fuel compacts arranged in three vertical stacks containing four compacts each. Figure 1 (right) displays a radial cross section view of a capsule illustrating the arrangement of the three compact stacks and showing the hafnium (Hf) shroud used to suppress the thermal neutron flux on the west side of the capsule [5].

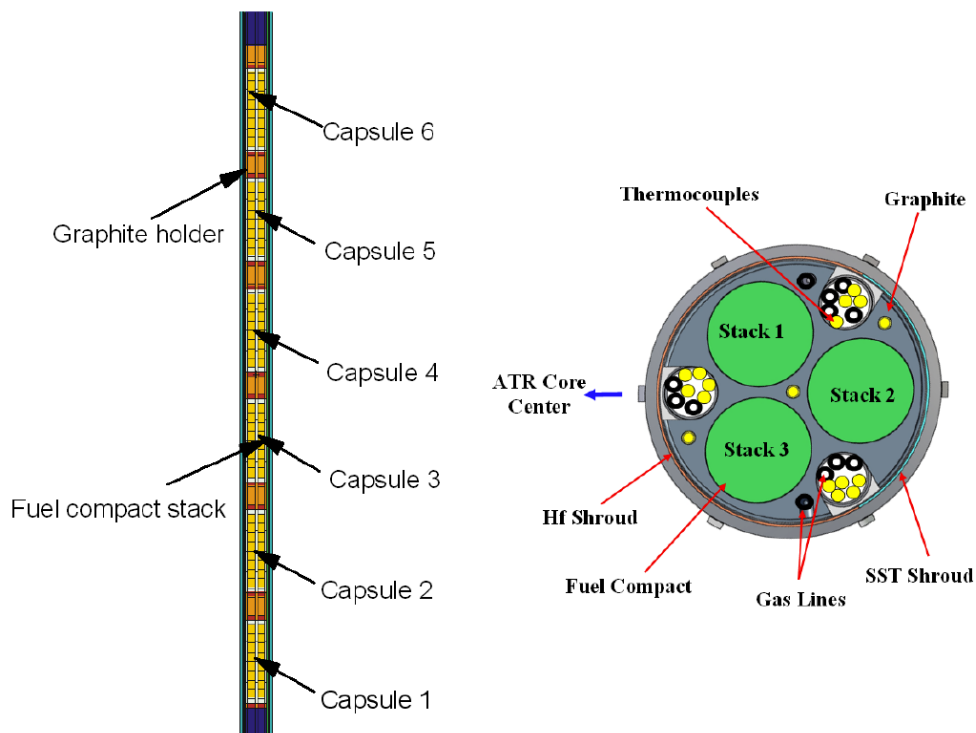


Figure 1. AGR-1 test train axial schematic (left) and radial cross section of a capsule (right).

The AGR-2 test train was nearly identical to the AGR-1 test train, but was designed for irradiation in the 38.1-mm-diameter B-12 (large B) position of the ATR. Five of the six AGR-2 capsules are 152.4 mm long and contain 12 fuel compacts arranged in three vertical stacks of four compacts. The compacts in AGR-2 Capsule 1 are different in dimension from the other AGR-2 compacts, and are not included in the analysis [6].

The AGR-3/4 experiment was placed in the northeast flux trap position in the ATR core. An axial view of the irradiation test train and two of the 12 capsules is shown in the side of Figure 2 (left). Four through tubes carry thermocouples and gas lines to each individual capsule. All 12 capsules have their

own gas mixture and gas supply and return line. Figure 2 (left) also represents the arrangement of capsules stacked together to form the experiment train. Each capsule has a stack of four fuel compacts in the center surrounded by three annuli of graphite and/or graphitic matrix material, as shown in the radial cut of the capsule Figure 2 (right) [7]. While 12 capsules were used in the AGR-3/4 experiment only a subset were used in this analysis because several capsules were not disassembled in time for the preparation of this report [8].

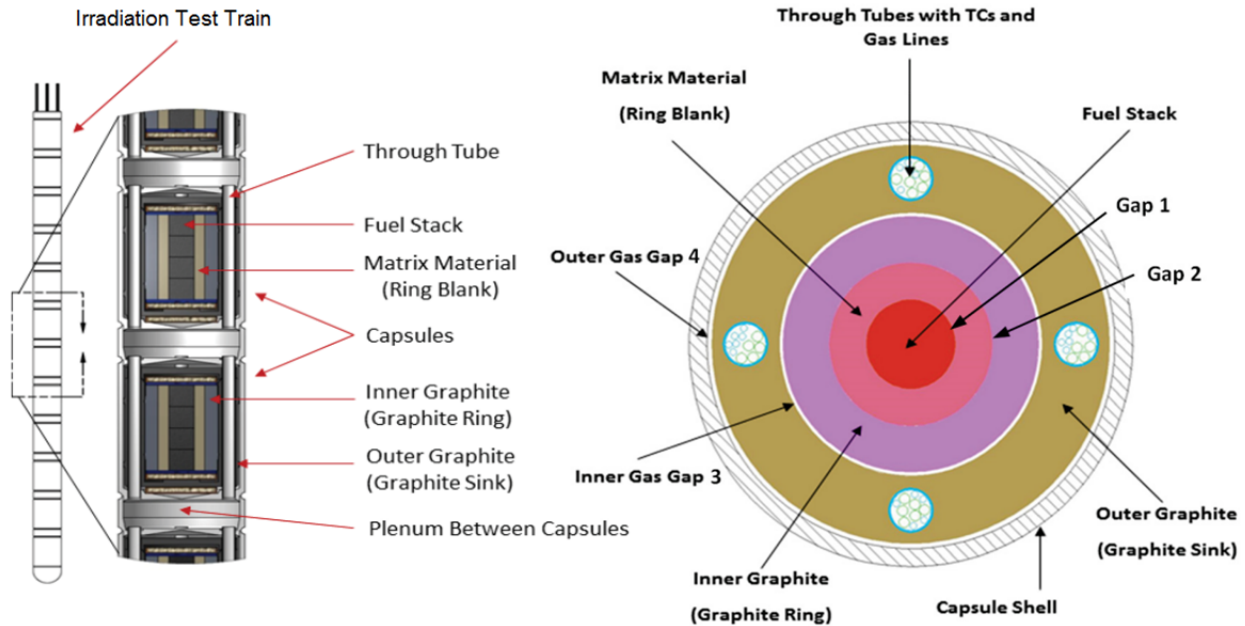


Figure 2. AGR-3/4 axial schematic (left) and radial cut of a capsule (right).

The AGC-2 experiment consisted of one fully instrumented capsule irradiated in the south flux trap of ATR. The capsule contained a specimen holder with six equally spaced channels around a single central channel. Each irradiation capsule is comprised of over 400 graphite specimens that are characterized before and after irradiation to determine the irradiation-induced material properties changes and life-limiting irradiation creep rate for each graphite grade. The AGC test train and irradiation capsules have the same general physical configuration to provide a consistent dose and applied mechanical stresses on compacts of similar graphite grades. While there are key machining and structural differences between capsules to change the irradiation temperature for the different capsules, the majority of the AGC design is identical for all capsules. A schematic of the AGC-2 test train is shown in Figure 3.

The AGC graphite compacts used in this analysis were located in the center channel or bottom half of the outer channels and did not receive any mechanical stress. These compacts were composed of A3 graphitic matrix material, which is the same material as the fuel compact matrix of the AGR experiments [2]. Fast neutron fluence for the AGC-2 compacts was interpolated from a calculated parabola fit based on their irradiation positions [9]. Several AGC-1 compacts composed of A3 graphitic matrix material were not included in the analysis because post-irradiation examination (PIE) measurements were unavailable.

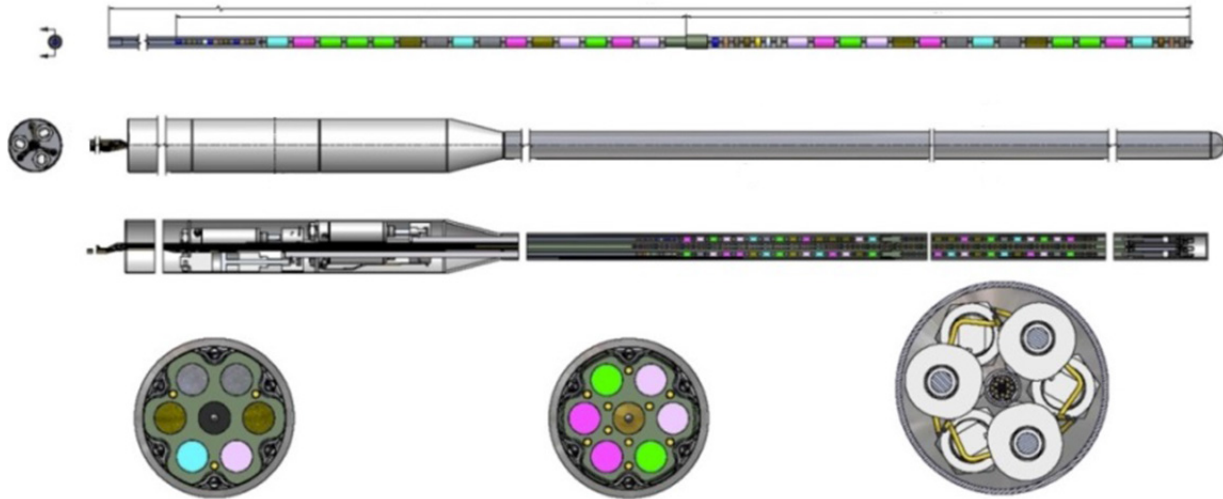


Figure 3. AGC-2 graphite compacts axial schematic (top) and radial cross section of a capsule (bottom).

3. DATA

Dimensional data for the AGR fuel compacts and AGC graphite compacts (length, diameter, and volume) were analyzed to determine whether significant changes were seen between the fabricated (FAB) and PIE measurements. All data utilized in this analysis originated from the Nuclear Data Management and Analysis System (NDMAS) 2.0 database [10].

3.1 Compact Diameter

AGC and AGR compact diameters do not vary much, with a range from 12.07 to 12.73 mm. Summarized diameter data by experiment is available graphically in Figure 4, and summary statistics are given in Table 1. Figure 4 is a boxplot by experiment for FAB and PIE diameter. The mean of the boxplot is indicated by a + symbol. The median is the middle line in the boxplot, with the 25th and 75th percentiles indicated at the ends of each box. The whiskers denote the minimum and maximum and encompass the range of the data. Note that each FAB boxplot is much smaller in range than the respective PIE boxplot.

Compact diameters are measured multiple times, with measurements at different axial regions; the number of replications is dependent upon the experimental test train. Results from a paired t-test indicate there is a statistically significant difference between FAB and PIE diameter by experiment. The PIE diameter measurement is always less than the FAB measurement.

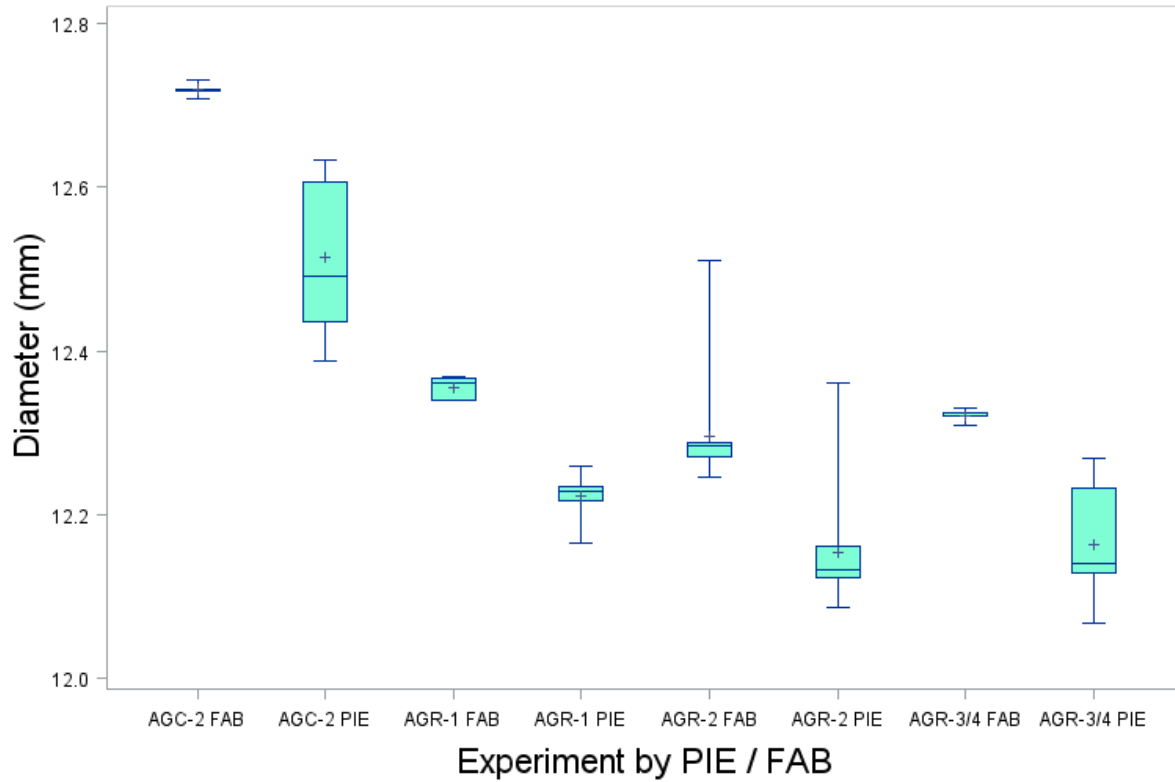


Figure 4. FAB and PIE diameter box plot for compacts included in this analysis by experiment.

Table 1. Summary statistics for measured FAB and PIE compact diameters included in this analysis by experiment. “N” represents the number of compacts analyzed from each experiment.

Variable Name	N	Mean	Standard Deviation	Minimum	Maximum
Experiment=AGR-1					
FAB Diameter	72	12.36	0.011	12.34	12.37
PIE Diameter	72	12.22	0.018	12.16	12.26
Experiment=AGR-2					
FAB Diameter	60	12.28	0.015	12.25	12.29
PIE Diameter	60	12.14	0.024	12.09	12.18
Experiment=AGR-3/4					
FAB Diameter	24	12.32	0.005	12.31	12.33
PIE Diameter	24	12.16	0.064	12.07	12.27
Experiment=AGC-2					
FAB Diameter	17	12.72	0.005	12.71	12.73
PIE Diameter	17	12.51	0.092	12.39	12.63

3.2 Compact Length

Compact lengths range from 6.25 to 25.3 mm, and are measured at FAB and PIE, as seen in Table 2. Measurement methods for FAB and PIE length differ. AGR FAB compact lengths represent a single measurement using a micrometer probe placed at the center of one end of the compact [11], [12], and [13]. AGC FAB length was measured at various positions with a micrometer [14].

AGR-1 and AGR-2 PIE lengths were measured using a machine vision system, with measurements taken at three orientations [15], [16]. PIE lengths for AGR-3/4 compacts were measured with a micrometer; only one measurement was taken on each compact [17]. AGC PIE lengths were measured at various positions with a Vernier caliper [18]. A box plot of length measurements is not included here because the relatively large range in compact lengths across experiments dominated the plot.

A paired t-test was employed to identify if there was a significant difference between FAB and PIE. The results of the paired t-test indicate a statistically significant difference between FAB and PIE length by experiment. The PIE measurement is almost always smaller than the FAB measurement, with five instances of length increasing out of 173 compacts. This indicates that the AGC and AGR compacts shrank in length.

Table 2. Summary statistics for measured FAB and PIE compact lengths based on the compacts included in this analysis. “N” represents the number of compacts analyzed from each experiment.

Variable Name	N	Mean	Standard Deviation	Minimum	Maximum
Experiment=AGR-1					
FAB length	72	25.12	0.09	24.94	25.30
PIE length	72	24.96	0.09	24.79	25.18
Experiment=AGR-2					
FAB length	60	25.15	0.03	25.11	25.22
PIE length	60	25.02	0.07	24.92	25.16
Experiment=AGR-3/4					
FAB length	24	12.51	0.02	12.47	12.55
PIE length	24	12.46	0.04	12.40	12.53
Experiment=AGC-2					
FAB length	17	6.32	0.01	6.30	6.34
PIE length	17	6.29	0.05	6.25	6.41

3.3 Compact Volume

Compact volumes for FAB and PIE were calculated from length and diameter, using the equation for the volume of a cylinder as seen in Equation (1).

$$\text{Volume of a Cylinder} = \pi * \left(\frac{1}{2} \text{diameter}\right)^2 * \text{length} \quad (1)$$

Calculated volume for a compact ranged from 762.05 to 6150.61 mm³. Due to this large range, a boxplot will not be provided as it does not provide any insight to the behavior of the AGR and AGC compact volume change. A summary of compact volume by experiment is provided in Table 3. As seen in Table 3, the AGR and AGC-2 compacts are becoming smaller in volume and hence denser; this may be due to the composition of the compacts, or the temperature and irradiation conditions experienced.

Table 3. Summary statistics for calculated FAB and PIE compact volume across experiments included in this analysis. “N” represents the number of compacts analyzed from each experiment.

Variable Name	N	Mean	Standard Deviation	Minimum	Maximum
Experiment=AGR-1					
FAB Volume	72	3011.63	6.07	2996.70	3025.56
PIE Volume	72	2929.04	10.36	2906.64	2955.31
Experiment=AGR-2					
FAB Volume	60	2976.43	6.02	2959.35	2988.24
PIE Volume	60	2894.49	12.47	2862.63	2912.78
Experiment=AGR-3/4					
FAB Volume	24	1491.77	2.39	1486.79	1496.44
PIE Volume	24	1447.58	13.79	1431.66	1474.23
Experiment=AGC-2					
FAB Volume	17	803.37	1.53	798.59	805.72
PIE Volume	17	773.75	8.28	762.06	785.81

3.4 Compact Explanatory Variables

The independent variables associated with AGR and AGC compact manufacturing includes matrix density, compact density, and fuel particle packing fraction. AGC-2 compacts were specifically included in the analysis to assess the effect of a packing fraction of zero. Additional variables considered for the AGR compacts include uranium loading and fuel particle diameter. Average uranium loading per compact was divided by compact volume to calculate uranium per unit volume for a compact. The fuel properties data were taken for AGR-1 from these reports: [19], [20], [21], [22], [23], [24], [25], and [26]. The fuel properties data were taken for AGR-2 from these reports: [27], [28], and [29]. The fuel properties data were taken for AGR-3/4 from these reports: [30], [31], and [32].

Other variables related to conditions in the experiential test trains that produce dimensional change include end of irradiation cumulative fast neutron fluence (n/m^2 , $E > 0.18$ MeV) and volume average time average temperature per compact (VATAT). The fast fluence data for AGR-1, -2, -3/4, and AGC-2 were taken from these respective reports: [33], [34], [35], and [36]. VATAT per compact for AGR -1, -2, -3/4, and AGC-2 were taken from these respective reports: [37], [38], [39], and [40]. Summary statistics for the independent variables across all experiments are recorded in Table 4.

Table 4. Summary statistics for explanatory variables utilized in the analysis across experiments.

Variable	Unit	N	Mean	Standard Deviation	Minimum	Maximum
Experiment = AGR-1						
Compact Packing Fraction	%	72	0.35	0	0.35	0.35
Fast Fluence/ 10^{25} ($E > 0.18$ MeV)	n/m^2	72	3.459	0.560	2.140	4.246
VATAT per Compact	Celsius	72	1018.300	39.394	931.421	1107.700
Average Uranium loading per compact volume	g/cm^3	72	3.03E-04	1.65E-06	3.00E-04	3.06E-04
Average TRISO Fuel Particle Diameter	μm	72	798.65	3.0807444	795.1	804

Table 4. (continued).

Variable	Unit	N	Mean	Standard Deviation	Minimum	Maximum
FAB Matrix Density	g/ cm ³	72	1.293	0.045	1.219	1.344
FAB Compact Density	g/ cm ³	72	1.818	0.033	1.766	1.881
Experiment = AGR-2						
Compact Packing Fraction	%	60	0.308	0.077	0.2	0.37
Fast Fluence/10 ²⁵ (E > 0.18 MeV)	n/m ²	60	3.102	0.417	1.941	3.526
VATAT per Compact	Celsius	60	1065.8	88.492	950.885	1261.750
Average Uranium loading per compact volume	g/ cm ³	60	3.26E-04	1.52E-04	3.19E-05	4.22E-04
Average TRISO Fuel Particle Diameter	μm	60	895.52	31.53	873.2	953
FAB Matrix Density	g/ cm ³	60	1.62	0.04	1.58	1.69
FAB Compact Density	g/ cm ³	60	2.087	0.032	2.037	2.122
Experiment = AGR-3/4						
Compact Packing Fraction	%	24	0.361	0.001	0.36	0.364
Fast Fluence/10 ²⁵ (E > 0.18 MeV)	n/m ²	24	3.628	1.527	1.195	5.286
VATAT per Compact	Celsius	24	1050.48	151.599	798.429	1260.59
Average Uranium loading per compact volume	g/ cm ³	24	3.02E-04	4.83E-07	3.01E-04	3.03E-04
Average TRISO Fuel Particle Diameter	μm	24	811.8	0	811.8	811.8
FAB Matrix Density	g/ cm ³	24	1.598	0.005	1.590	1.608
FAB Compact Density	g/ cm ³	24	2.010	0.004	2.003	2.017
Experiment = AGC-2						
Compact Packing Fraction	%	17	0	0	0	0
Fast Fluence/10 ²⁵ (E > 0.18 MeV)	n/m ²	17	3.729	1.469	1.868	5.804
VATAT per Compact	Celsius	17	573.687	87.187	430.669	694.388
Average Uranium loading per compact volume	g/ cm ³	17	0	0	0	0
Average TRISO Fuel Particle Diameter	μm	17	0	0	0	0
FAB Matrix Density	g/ cm ³	17	1.541	0.148	1.406	1.797
FAB Compact Density	g/ cm ³	17	1.541	0.148	1.406	1.797

4. ANALYSIS

Changes in compact dimensions are important because of the impact on the gas gaps used to control temperature. Compact shrinkage affects temperature control and other variables that are important to the AGR experiment. In AGR and AGC there exist a greater number of capsules than were included in this analysis, but due to technical difficulties and the design of the analysis this number has been reduced. As such, across AGR and AGC there exist 19 capsules available for inclusion in the analysis. Each capsule differs in composition and irradiation exposure; because of the many groups that needed to be compared, the preferred statistical approach is to use a multiple comparisons test to identify significant differences between group means, assuming a normal distribution [41]. The Duncan Multiple Range Test (DMRT)

was chosen for its sensitivity in identifying a significant difference among groups [42]. When the DMRT groups overlap, this indicates that the different DMRT groups are not significantly different from one another and are in the same cohort. The number of DMRT groups changes per each analysis, with as few as one DMRT group, or as many as 19, for this analysis.

After capsule groups have been identified to remain in the cohort, models are constructed to explain the percent of dimensional change. The percent of change was chosen as it is unit-less and allows measurements for different experiments to be relatable. The seven variables in Table 4 were all considered for use in the regression, in addition to fast fluence squared. Fast fluence squared was considered as a variable in the regression due to it consistently performing well in predicting dimensional change when compared alongside multiple second order variables.

Because certain statistical tests will always define models with more variables as better-performing, it is considered best practice to limit the number of independent variables used in the models. In order to determine the most appropriate number of variables for inclusion in the model, multiple statistical tests were considered. The models created are of the form in Equation (2).

$$Y = B_0 + B_1X_1 + B_2X_2 + B_3X_3 + B_4X_4 \quad (2)$$

Here B_0 is the intercept; B_1, B_2, B_3 , and B_4 are the explanatory variable coefficients and X_1, X_2, X_3 , and X_4 are the observed variable values. The Y represents the dimensional variable we are trying to describe, or the dependent variable. The best performing model, as determined by several statistical factors, was selected from a pool of several hundred regression model candidates for each dimension. The regressions models are based upon the range of the data available and should not be extrapolated beyond the range of the data provided.

As validation of the selected model, a bootstrap simulation was completed [43]. Each bootstrap had a 60/40 partition, where 40% of the data was randomly removed, and then several hundred candidate models were built based on the remaining 60% of the data. This process was repeated 5,000 times with each individual iteration retaining the best performing model. Consistent results from the full-data model fit and a majority of the bootstrap indicate a robust and well-performing model. All statistical analyses were completed in SAS 9.4 [44].

The statistical methods outlined above will be implemented to identify variables that are significantly impacting dimensional change. The variables of dimensional change considered are compact diameter, length and volume all of which are measured in mm. The following sections 4.1-4.3 will cover the statistical tests by dimension and basic output.

4.1 Change in Compact Diameter

The first dimension considered was diameter, with the percent change in compact diameter calculated from Equation (3).

$$\text{percent change in Diameter} = \frac{\text{PIE Diameter} - \text{FAB Diameter}}{\text{FAB Diameter}} * 100 \quad (3)$$

The percent change in diameter is averaged for each capsule. A DMRT was implemented to detect if any capsules are significantly different from other capsules. When capsules are significantly different they need to be excluded from the cohort because of the confounding effects they may cause in the analysis. The DMRT group column in Table 5 is utilized to interpret the results; means with the same letter are not significantly different from each other. When different DMRT groups overlap, a continuum of non-significantly different percent change in diameter exists and indicates that all capsules belong to the same cohort. The results for the DMRT of percent change in diameter are displayed in Table 5.

Table 5. Results of a Duncan's Multiple Range Test for percent change in diameter.

DMRT group		Mean % Change	N	Group
	A	-0.514	4	AGR-3/4 Capsule 12
B	A	-0.701	4	AGR-3/4 Capsule 1
B	C	-0.953	12	AGR-1 Capsule 4
	C	-0.987	12	AGR-2 Capsule 6
	C	-1.016	12	AGR-2 Capsule 5
	C	-1.055	12	AGR-1 Capsule 5
	C	-1.056	12	AGR-1 Capsule 3
	C	-1.058	12	AGR-1 Capsule 6
	C	-1.089	12	AGR-1 Capsule 2
	C	-1.150	12	AGR-2 Capsule 3
D	C	-1.208	12	AGR-1 Capsule 1
D	E	-1.429	12	AGR-2 Capsule 2
D	E	-1.434	4	AGR-3/4 Capsule 10
D	E	-1.474	4	AGR-3/4 Capsule 8
	E	-1.579	4	AGR-3/4 Capsule 3
	E	-1.607	17	AGC-2
	F	-1.949	4	AGR-3/4 Capsule 7
AGR-2 Capsule 4 is retained in the analysis, but is not reported per Cooperative Research and Development Agreement.				

All measurements of diameter are decreasing from FAB to PIE. Groups A, B, C, D and E are all overlapping, indicating that they are all from the same cohort. The DMRT Grouping F in Table 5 indicates that AGR-3/4 Capsule 7 is significantly different from all the other capsules; however, the relative difference in diameter between Groups F and E is only 0.34%. Additionally, there are no experimental differences between AGR-3/4 Capsule 7 and the other AGR-3/4 capsules; and the difference of 0.34% change in diameter is relatively small. Hence the AGR-3/4 Capsule 7 is retained in the analysis and in the same cohort as the other capsules. AGC-2 is in DMRT Group E, along with three AGR-3/4 capsules (3, 8, and 10) and AGR-2 Capsule 2. This is additional grounds for inclusion of the 17 AGC-2 observations in the analysis.

The 173 compacts were then regressed for percent change in diameter. The selections of variables that have a significant impact on the percent change in diameter, as calculated from Equation (3), are displayed in Table 6.

Table 6. The top-performing regression with four variables, to predict percent change in diameter.

Variable	Parameter Estimates	Standard Error	t Value	Pr > t
VATAT (°C)	-2.12E-03	9.78E-05	-21.68	<.0001
TRISO Fuel Particle Diameter (μm)	1.02E-03	1.04E-04	9.8	<.0001
Compact Packing Fraction (%)	1.54	0.21	7.47	<.0001
(Fast Fluence/10 ²⁵) ² (n/m ²) ²	-0.02	2.42E-03	-9.99	<.0001

The parameter estimates from Table 6 were substituted into B_0 , B_1 , B_2 , B_3 , and B_4 in Equation (2) to generate the resulting model in Equation (4).

$$\begin{aligned} \text{Percent Change in Diameter} = & -2.12\text{E-}03 * \text{VATAT per Compact} + \\ & 1.02\text{E-}03 * \text{TRISO Fuel Particle Diameter} + 1.54 * \text{Compact Packing Fraction} + \\ & -0.02 * (\text{Fast Fluence}/10^{25})^2 \end{aligned} \quad (4)$$

In this case, the intercept was not calculated and as such $B_0 = 0$. This was because the intercept was not statistically significant, with a p-value of 0.64, and when removed the adjusted r-squared increased from 79% to 98%. The fit for percent change in diameter was then bootstrapped for assurance that a robust model was selected with 4,299 iterations out of 5,000 selecting the variables listed in Table 6. Finally, the predicted change in diameter calculated from Equation (4) was plotted against the observed change in diameter, as displayed in Figure 5.

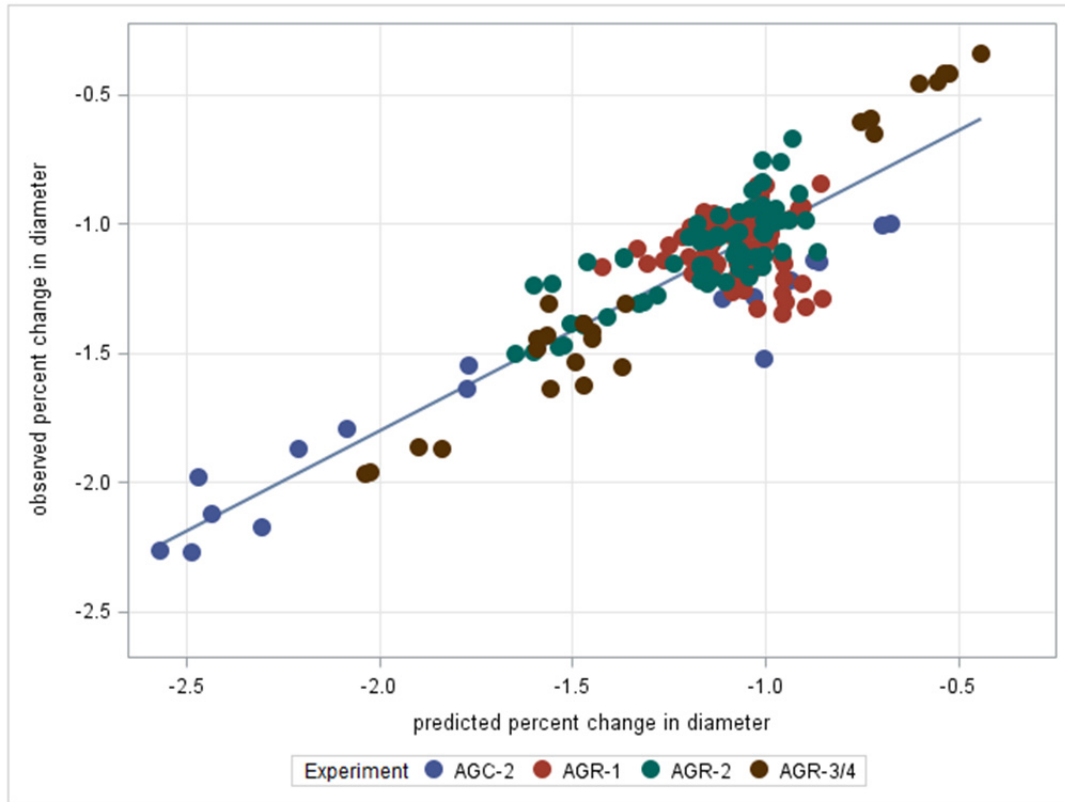


Figure 5. Observed regressed by predicted percent change in diameter by compact.

The variance in Figure 5 does not display any pattern, and the residual is normally distributed, with an adjusted r-square of 98% for the regression. The overall regression model and each variable are statistically significant. When the regression of observed-to-predicted percent change in diameter (Figure 5) is done by experiment (four separate regressions), the slope ranges from 0.99 to 1.06, which is a very narrow range. These indicators show that the chosen model does not differ much by experiment and is a robust choice for describing percent change in diameter.

4.2 Change in Compact Length

The next dimensional change that was analyzed is compact length. For comparison, each compact has its percent change in length calculated as from Equation (5).

$$\text{percent change in Length} = \frac{\text{PIE Length} - \text{FAB Length}}{\text{FAB Length}} * 100 \quad (5)$$

The values from Equation (5) are averaged per capsule, as seen in Table 7. A DMRT analysis of compact length was carried out to ascertain the inclusion of experimental capsule groups in the cohort. Results from the DMRT percent change in length are contained in Table 7. The DMRT group columns can be used to interpret the results; means with the same letter are not significantly different from each other. AGC-2 is in DMRT Group B and C. This means that AGC-2 is not significantly different from all the capsules in DMRT Groups B and C; this includes all of the capsules in AGR-1, most of -2, and most of -3/4. The DMRT Groups all overlap, signifying that none of the capsules exhibit extremely different percent change in length by capsule. Thus based on Table 7 none of the capsules need to be excluded from the cohort.

Table 7. Results of a Duncan's Multiple Range Test for percent change in fabricated and post-irradiation examination length.

DMRT group		Mean % Change	N	Group
	A	-0.0233	4	AGR-3/4 Capsule 7
	A	-0.0724	4	AGR-3/4 Capsule 8
B	A	-0.282	12	AGR-2 Capsule 3
B	C	-0.4911	4	AGR-3/4 Capsule 12
B	C	-0.5105	12	AGR-1 Capsule 3
B	C	-0.5107	12	AGR-1 Capsule 4
B	C	-0.5182	17	AGC-2
B	C	-0.5608	12	AGR-2 Capsule 6
B	C	-0.5797	12	AGR-1 Capsule 2
	C	-0.6185	4	AGR-3/4 Capsule 10
	C	-0.6215	12	AGR-2 Capsule 5
	C	-0.6687	12	AGR-1 Capsule 5
	C	-0.6902	4	AGR-3/4 Capsule 3
	C	-0.7189	12	AGR-1 Capsule 6
	C	-0.7428	4	AGR-3/4 Capsule 1
	C	-0.7786	12	AGR-1 Capsule 1
	C	-0.7997	12	AGR-2 Capsule 2
AGR-2 Capsule 4 is retained in the analysis, but is not reported per Cooperative Research and Development Agreement.				

Percent change in length was regressed; however, results from the regression and bootstrap were not consistent. A transformation of the percent change in length to the natural log (ln) of percent change in length was analyzed. Since the percent change in length has negative and positive observations, the natural logarithm of one minus the percent change in length was implemented, as seen in Equation (6). The percent change was not multiplied by 100, as this may cause errors in the regression when the mean of the variable is much greater than its range. The best performing regression from Equation (6) is presented in Table 8.

$$\ln(\text{percent change in Length}) = \ln\left(1 - \left(\frac{\text{PIE Length} - \text{FAB Length}}{\text{FAB Length}}\right)\right) \quad (6)$$

Table 8. The top performing regression with four variables for natural log of the transformed percent change in length.

Variable	Parameter Estimates	Standard Error	t Value	Pr > t
Intercept	-0.003	0.001	-2.4	0.0177
Fast Fluence/ 10^{25} (n/m ²)	0.009	8.46E-04	10.62	<.0001
(Fast Fluence/ 10^{25}) ² (n/m ²) ²	-0.002	1.20E-04	-13.09	<.0001
Packing Fraction (%)	0.020	0.002	9.97	<.0001
TRISO Fuel Particle Diameter (μm)	-1.1E-05	9.49E-07	-11.92	<.0001

The parameter estimates from Table 8 are substituted into B_0 , B_1 , B_2 , B_3 , and B_4 in Equation (2) to get the resulting model:

$$\begin{aligned} \text{Natural Log of the Transformed Percent Change in Length} = \\ -0.003 + 0.009 * \text{Fast Fluence}/10^{25} + -0.002 * (\text{Fast Fluence}/10^{25})^2 + \\ 0.02 * \text{Packing Fraction} + -1.1\text{E-}05 * \text{TRISO fuel particle diameter} \end{aligned} \quad (7)$$

A bootstrap analysis was then used for verification of model selection, with the top performing regression model selecting the variables in Equation (7) 4,497 out of 5,000 iterations. Figure 6 shows the regression of the predicted to the observed natural log of the transformed percent change in length. The residuals are normally distributed and without a noticeable trend, which is a desirable result. The adjusted r-square for the regression is 74%, and the overall regression model and coefficient for each variable are statistically significant. When the regression of observed by predicted natural log of the transformed percent change in length is completed by experiment (four separate regressions) rather than an overall model (one regression), the slope differs by each experiment. The slopes by experiment are all positive and range from 0.29 to 0.91, which is a narrow range. These indicators lead to the conclusion that the model in Table 8 is very robust and does not vary much by experiment.

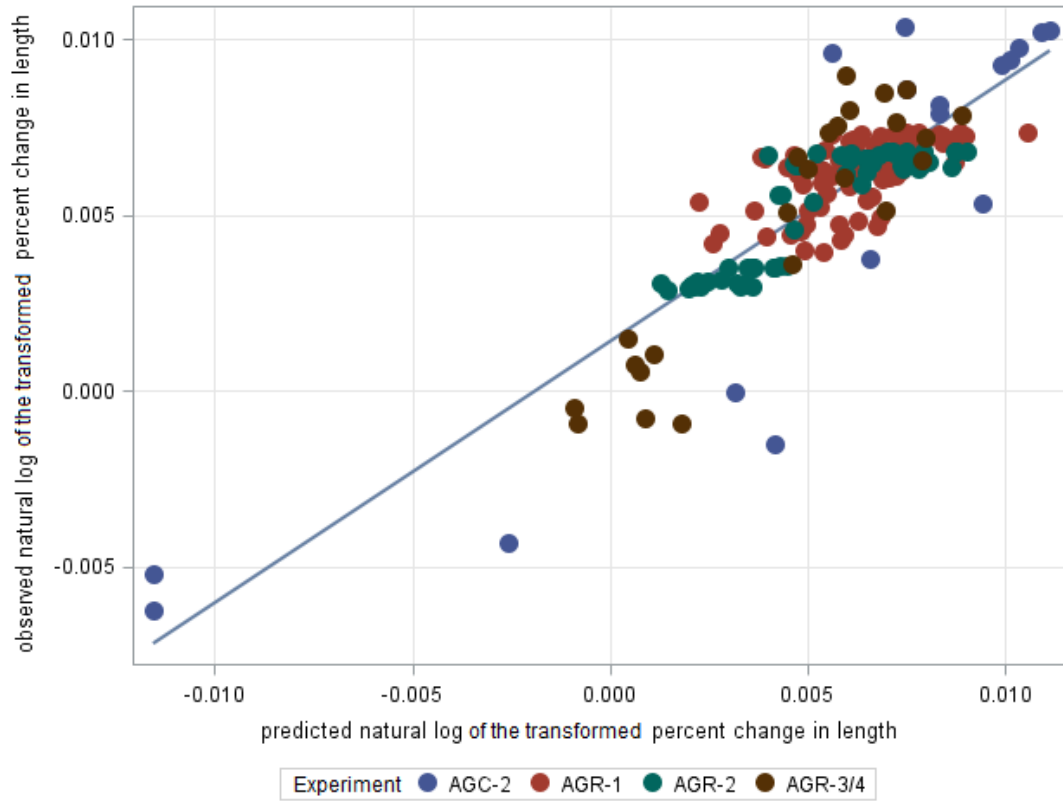


Figure 6. Observed plotted against predicted natural log of the transformed percent change in length.

4.3 Change in Compact Volume

The last dimension analyzed is volume. Because the volume is calculated from compact length and diameter, and a DMRT was completed on each dimension, a DMRT for volume will not be presented. Percent change in volume was calculated from Equation (8).

$$\text{percent change in volume} = \frac{\text{PIE volume} - \text{FAB volume}}{\text{FAB volume}} * 100 \quad (8)$$

However, a model that performed consistently well was not located, so the Ln of percent change in volume, as seen in Equation (9) was implemented as the dependent variable. The numerator to the percent change in volume was negated from the previous equation, as a negative percent change cannot have an Ln applied.

$$\text{Ln}(\text{percent change in volume}) = \text{Ln} \left(\frac{\text{FAB volume} - \text{PIE volume}}{\text{FAB volume}} * 100 \right) \quad (9)$$

Equation (9) was then regressed using the selection of variables from Table 4. All 173 compacts decreased in total volume. The best performing model out of several hundred candidate models, with four or less variables, is displayed in Table 9.

Table 9. The top performing regression with four variables for natural log of percent change in volume.

Variable	Parameter Estimate	Standard Error	T - Value	Pr > t
Intercept	0.412	0.122	3.37	0.0009
Compact Packing Fraction (%)	-0.962	0.161	-5.98	<.0001
VATAT per compact (°C)	0.002	0.000	18.34	<.0001
FAB Compact Density (g/ cm ³)	-0.233	0.082	-2.84	0.0051
TRISO Fuel Particle Diameter (μm)	-9.83E-04	8.19E-05	-12	<.0001

A bootstrap simulation was then completed, with the model from Table 9 being selected 2804 times out of 5000. While the bootstrap results were not as strong as the previous two dimensional models this was the best performing for this dimension. This may be related to percent volume change being calculated from length and diameter. There is a very strong correlation between volume and diameter, with an adjusted r-squared of 0.82. Contrastingly, the relationship between length and volume is very weak, with an adjusted r-square of 0.004. While there are compacts with increasing length, there are no compacts with increasing diameter, and the behavior of volume more closely follows that of diameter. As such the variables selected in the volume regression might be confounded by the fact it is calculated from the two measurements, rather than directly being measured.

Finally, a model is produced from substituting the parameter estimates from Table 9 into Equation (2), which is used to calculate the predicted log of percent change in volume. The predicted log percent change in volume is regressed onto the observed value in Figure 7.

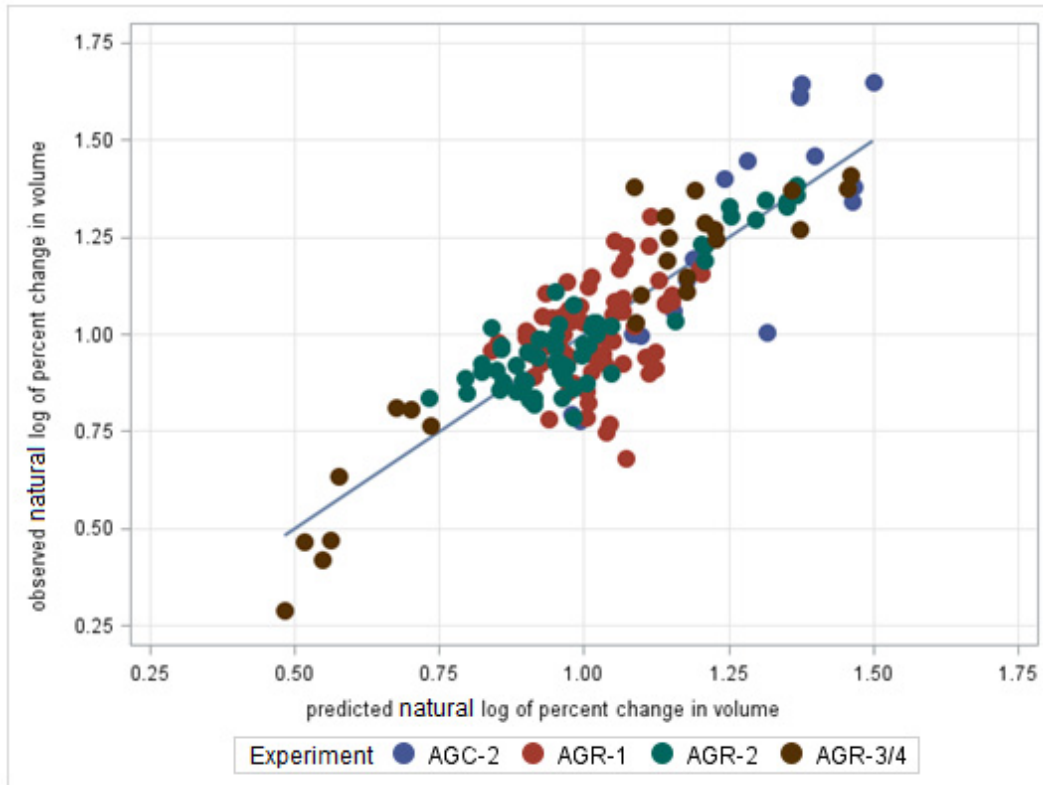


Figure 7. The observed by predicted natural log of percent change in volume.

The residuals for Figure 7 are normally distributed, and without distinct behavior. The adjusted r-squared was 0.72, for the overall model. A regression was completed of the observed Ln of percent change volume to the predicted for each experiment (four separate regressions). This resulted in a range of slope from 0.47 to 1.5, and shows that each experiment behaved similarly for the regression model in Table 9.

5. CONCLUSION AND DISCUSSION

The coefficient values for each variable from the three dimensional change models are shown in Table 10. The Total Use column indicates the number of times a variable was selected in the regression models. The percent change in volume is highly correlated (greater than 99%) with percent change in compact density by experiment. Thus, it is unusual that the compact density was only selected once in the regression models. One reason for this might be because compact density is calculated for the entire compact, and as such includes the fuel particles, which are known not to change in dimension.

Table 10. Regression coefficients for change in length, diameter, and volume.

Variable	Regression Model			
	% Change in Diameter	Ln of % Change in Length	Ln of % Change in Volume	Total Use
Compact Packing Fraction (%)	1.54	0.02	-0.962	3
FAB Matrix Density (g/ cm ³)				0
Fast Fluence/10 ²⁵ (E > 0.18 MeV) (n/m ²)		0.009		1
(Fast Fluence/10 ²⁵) ² (n/m ²) ²	-0.02	-0.002		2
VATAT per Compact (°C)	-2.12E-03		0.002	2
FAB Compact Density (g/ cm ³)			-0.233	1
Average Uranium loading per compact volume (g/ cm ³)				0
TRISO Fuel Particle Diameter (μm)	1.02E-03	-1.10E-05	-9.83E-04	3

Matrix density was not selected in any dimensional change regression model. The dimensional change is thought to come from molecular changes in the matrix during irradiation. The lack of matrix density in a model indicates that based upon this dataset and analysis it is not statistically significant in predicting dimensional change.

The average uranium loading per unit volume for a compact was also never selected in any of the dimensional change models. This might be because uranium loading is related to other parameters such as kernel size (TRISO Fuel Particle Diameter), kernel density, kernel composition (UO₂ or UCO), and/or packing fraction. Kernel size is directly related to the TRISO Fuel Particle Diameter because the biggest contributor to particle size is the kernel size. Based on the results of this analysis it is more likely that the relationship between dimensional change and uranium loading per unit volume is weaker than that of dimensional change and packing fraction or particle diameter.

The packing fraction, matrix density, fast fluence, temperature, and particle diameter are all chosen one or more times as seen in Table 10. All three regression models for dimensional change selected the TRISO fuel particle diameter and packing fraction. The selection of particle diameter in dimensional change was seen before in, Goeddel et al. who advocated that fuel particle diameter directly relates to dimensional stability [45].

Particle diameter was measured for each lot of particles. Each capsule contains particles from one fuel particle lot, and hence has a fixed average particle diameter. In AGR-3/4, all capsules have the same average particle diameter. AGC-2 capsules do not contain fuel particles; hence they are all reported as having particle diameter 0. Because of this, confounding between particle diameter and capsule occurs.

Therefore, the selection of particle diameter as a significant parameter in the regression models may be due to factors unique by capsule.

Furthermore, the selection of packing fraction in the regression of diameter and volume might also be confounded with the experiment. Packing fraction was reported to two significant figures at the experiment level for AGR-1, -2, and AGC-2. While the AGR-3/4 packing fractions were reported with more precision for each compact, the values all round to 0.36. Hence, there are four discrete packing fractions, one for each experiment. Due to the discrete nature of packing fraction, its selection in the model is either indicating that the packing fraction, or factors unique to the experiment, is significant.

The variables selected into the three regression models were chosen empirically and without human bias. Data analysis results indicate that packing fraction, compact density, fast fluence, VATAT, and fuel particle diameter are highly statistically significant variables in explaining dimensional changes. As a result of the methods employed in this analysis, it is highly likely that these models will remain statistically significant even if additional data are gathered.

6. REFERENCES

- [1] L. Tan, T. R. Allen, J. D. Hunn and J. H. Miller, "EBSD for microstructure and property characterization of the SiC-coating in TRISO fuel particles," *Journal of Nuclear Materials*, vol. 372, no. 2-3, pp. 400-404, 2008.
- [2] W. Windes, W. D. Swank, D. T. Rohrbaugh, and D. L. Cottle, *AGC-2 Specimen Post-Irradiation Data Package Report*, INL/EXT-15-36244, August 2015.
- [3] Entegris, "Properties and Characteristics of Graphite," Entegris, Billerica, 2013.
- [4] A. J. Wickham, "Treatment Options for the Disposal Of Radioactive Graphite Wastes," 2014. [Online]. Available: https://www.iaea.org/NuclearPower/Downloadable/Meetings/2015/2015-02-25-02-27-NPTDS/day2/B04-Treatment_Options_for_i-Graphite.pdf. [Accessed 23 December 2015].
- [5] B. P. Collin, *AGR-1 Irradiation Test Final As-Run Report*, INL/EXT-10-18097, January 2015.
- [6] B. P. Collin, *AGR-2 Irradiation Test Final As-Run Report*, INL/EXT-14-32277, July 2014.
- [7] B. P. Collin, *AGR-3/4 Irradiation Test Final As-Run Report*, INL/EXT-15-35550, June 2015.
- [8] J. Stempien, F. Rice, P. Winston, J. Harp, AGR-3/4 Irradiation Test Train Disassembly and Component Metrology First Look Report, INL/EXT-16-38005, March 2016.
- [9] L. L. Tuckett, Reactor Physics Projections for the AGC-2 Experiment Irradiated in the ATR South Flux Trap," ECAR-1050, Rev. 0, 2010.
- [10] L. Hull, *NDMAS System and Process Description*, INL/EXT-12-27594, October 2012.
- [11] P. Demkowicz, L. Cole, S. Ploger, P. Winston, "AGR-1 Irradiated Test Train Preliminary Inspection and Disassembly First Look," INL/EXT-10-20722, January 2011.
- [12] K. L. Kynaston, *AGR-3/4 Metrology*, HFEF-LI-0072, Rev. 1, August 2015.
- [13] K. L. Kynaston, *AGR-2 Metrology*, HFEF-LI-0032, Rev. 2, November 2014.
- [14] W.E. Windes; P.L. Winston; W.D. Swank, "AGC-2 Disassembly Report," INL/EXT-14-32060, May 2014.
- [15] P. Demkowicz, L. Cole, S. Ploger, P. Winston, "AGR-1 Irradiated Test Train Preliminary Inspection and Disassembly First Look," INL/EXT-10-20722, January 2011.

- [16] K. L. Kynaston, *AGR-2 Metrology*, HFEF-LI-0032, Rev. 2, November 2014.
- [17] K. L. Kynaston, *AGR-3/4 Metrology*, HFEF-LI-0072, Rev. 1, August 2015.
- [18] W.E. Windes; P.L. Winston; W.D. Swank, "AGC-2 Disassembly Report," INL/EXT-14-32060, May 2014.
- [19] J. D. Hunn, F. C. Montgomery and P. J. Pappano, "Data Compilation for AGR-1 Baseline Compact Lot LEU01-46T-Z," ORNL/TM-2006/507, Rev. 0, August 2006.
- [20] J. D. Hunn, R. A. Lowden, "Data Compilation for AGR-1 Baseline Coated Particle Composite LEU01-46T," ORNL/TM-2006/019, Rev. 1, April 2006.
- [21] J. D. Hunn, R. A. Lowden, "Data Compilation for AGR-1 Variant 1 Coated Particle Composite LEU01-47T," ORNL/TM-2006/020, Rev. 1, April 2006.
- [22] J. D. Hunn, F. C. Montgomery and P. J. Pappano, "Data Compilation for AGR-1 Variant 1 Compact Lot LEU01-47T-Z," ORNL/TM-2006/508, Rev. 0, August 2006.
- [23] J. D. Hunn, R. A. Lowden, "Data Compilation for AGR-1 Variant 2 Coated Particle Composite LEU01-48T," ORNL/TM-2006/021, Rev. 1, May 2006.
- [24] J. D. Hunn, F. C. Montgomery and P. J. Pappano, "Data Compilation for AGR-1 Variant 2 Compact Lot LEU01-48T-Z," ORNL/TM-2006/509, Rev. 0, August 2006.
- [25] J. D. Hunn, R. A. Lowden, "Data Compilation for AGR-1 Variant 3 Coated Particle Composite LEU01-49T," ORNL/TM-2006/022, Rev. 0, May 2006.
- [26] J. D. Hunn, F.C. Montgomery P.J. Pappano, "Data Compilation for AGR-1 Variant 3 Compact Lot LEU01-49T-Z," ORNL/TM-2006/510, Rev. 0, August 2006d.
- [27] J. D. Hunn, F.C. Montgomery, P.J. Pappano, "Data Compilation for AGR-2 B&W UO2 Compact Lot LEU11-OP2-Z", ORNL/TM-2010/055, Rev. 0, February 2010.
- [28] J. D. Hunn, F.C. Montgomery, P.J. Pappano, "Data Compilation for AGR-2 UCO Variant Compact Lot LEU09-OP2-Z", ORNL/TM-2010/017, Rev. 0, February 2010.
- [29] J. D. Hunn, F.C. Montgomery, P.J. Pappano, "Data Compilation for AGR-2 PBMR UO2 Compact Lot LEU08-OP3-Z", ORNL/TM-2010/070, Rev 0, 2010.
- [30] J. D. Hunn, "Data Compilation for AGR-3/4 Designed-To-Fail (DTF) Fuel Particle Batch LEU03-07DTF", ORNL/TM-2011/109, Rev. 0, April 2011.
- [31] J. D. Hunn, "Data Compilation for AGR-3/4 Driver Fuel Coated Particle Composite LEU03-09T", ORNL/TM-2007/019, Rev. 0, March 2007.
- [32] J. D. Hunn, "Data Compilation for AGR-3/4 Designed-to-Fail (DTF) Fuel Compact Lot (LEU03-10TOP2/LEU03-07DTF-OP1)-Z", ORNL/TM-2011/124, Rev. 0, June 2011.
- [33] J. W. Sterbentz, *JMOCUP as-Run Daily Depletion Calculation for the AGR-1 Experiment in ATR B-10 Position*, ECAR-958, Rev. 2, August 2013.
- [34] D. A. Petti, *JMOCUP as-run Daily Depletion Calculation for the AGR-2 Experiment in ATR B-12 Position*, ECAR-2066, Rev. 2, January 2015.
- [35] J. W. Sterbentz, *JIMOCUP as-run Daily Physics Depletion Calculation for the AGR-3/4 TRISO Particle Experiment in ATR Northeast Flux Trap*, ECAR-2753, Rev. 1, 2015.
- [36] L. L. Tuckett, Reactor Physics Projections for the AGC-2 Experiment Irradiated in the ATR South Flux Trap," ECAR-1050, Rev. 0, 2010.

- [37] G. L. Hawkes, *AGR-1 Daily As-run Thermal Analyses*, ECAR-968, Rev. 4, 2014.
- [38] J. T. Maki, *AGR-2 Daily As-Run Thermal Analysis*, ECAR-2476, Rev. 0, 2014.
- [39] M. E. Davenport, *AGR-3/4 Daily As-Run Thermal Analyses*, ECAR-2807, Rev. 0, 2015.
- [40] L. L. Tuckett, *Thermal Evaluations for AGC-2 Experiment*, ECAR-1166, Rev. 2, 2010.
- [41] R. Parsad, "Multiple Comparison Procedures," I.A.S.R.I., New Delhi.
- [42] D. B. Duncan, "Multiple Range and Multiple F Tests," *Biometrics*, Vol. 11, No. 1, 1955, pp. 1-42.
- [43] B. Efron, "Bootstrap Methods: Another Look At The Jackknife," *The Annals of Statistics*, Vol. 7, No. 1, 1977, pp. 1-26.
- [44] SAS Institute Inc., "SAS 9.4 Help and Documentation," SAS Institute Inc., Cary, 2002-2004.
- [45] V. W. Goeddel, G. R. Tully, R. A. Meyer, "The Use of Graphite in High-Temperature Nuclear Fuel Elements," *Proceedings of the Fifth Conference on Carbon*, Vol 2, 1963, pp. 347-377.